AIAA AVIATION Forum
17-21 June 2019, Dallas, Texas
AIAA Aviation 2019 Forum

10.2514/6.2019-3536

Numerical Simulations of Asymptotic Theory for Distributed Roughness

Madeline N. McMillan*, Edward B. White†
Texas A&M University, College Station, Texas, 77843

Various experiments and numerical simulations have demonstrated that distributed roughness exhibits a 'shielding effect' whereby transition due to large-amplitude roughness elements within the distribution occurs at a higher Re_{kk} than if those elements were positioned on an otherwise flat surface. While this effect has been observed, it has not yet been captured in a theoretical model that could predict shielding effectiveness in new situations. As a first approximation, triple-deck asymptotic theory will be applied to simplified two-dimensional distributed roughness using a no-shear boundary condition applied at $y = 0$ over dips in the surface geometry. Results of this approach will be compared to equivalent no-slip conditions to assess the usefulness of this modeling approach.

I. Introduction

The ability to predict transition on an aerodynamic surface enhances engineers' ability to predict and reduce viscous drag. An important mechanism in the transition process is the receptivity of the boundary-layer to disturbances. It is well known that surface roughness has a large effect on transition. Two-dimensional roughness and, to a lesser extent, three-dimensional discrete (isolated) roughness, is fairly well understood through the lens of a critical roughness height, Re_k, which allows the prediction of transition [1].

Extending knowledge to three-dimensional, randomly distributed roughness fields has proved challenging. Although appealing as an incremental approach, analyzing the field as if it was a collection of discrete roughnesses has failed to yield useful progress. Distributed roughness is inherently different from discrete roughness in that the boundary layer does not interact with each element separately but, apparently, with the entire field.

Many experimentalists, beginning with Nikuradse [2] have investigated distributed roughness fields by testing with sandpaper roughness. An experiment by Reshotko and Leventhal [3] searched for an inflection point to appear in the boundary layer velocity profile moving above sandpaper roughness as this would destabilize Tollmien-Schlichting waves. However, they found only an outward displacement of the Blasius profile. Separately, Kendall [4] saw that disturbance energy was decreased when distributed roughness was added near a discrete element. That is, changing a large discrete element to be part of a roughness field reduced its impact on the flow. This is evidence of the shielding effect, but it was not recognized as such during the time.

More recent work has explicitly studied how shielding by distributed roughness diminishes the apparent impact of single discrete roughness elements. Drews et al. [5] conducted a DNS study on a distributed roughness that had previously been studied by Downs and White [6], and found that removing small amplitude roughness from around larger amplitude roughness caused disturbance energy to increase. Kuester and White [7] confirmed this finding and observed that distributed roughness around a discrete roughness element reduced disturbance amplitude and could move the transition location backwards. McMillan et al. [8] found that discrete roughness elements in a distributed roughness field could be extended to a larger Re_k without causing transition than without the surrounding distributed roughness.

One conceptual model for how shielding occurs is to imagine that the flow responds to distributed roughness by shifting out above the smaller elements such that the larger elements affect the flow at lower amplitude than they would in isolation. This is consistent with Reshotko and Leventhal's findings and the other references cited above. To model this, one approach could be to select an effective surface height above the small elements that reduces the height of the large elements. This raises the question: Where is this effective surface and can we predict it such that we can better predict transition from a field of distributed roughness? The objective of this work is to evaluate the effectiveness of a slip surface at $y = 0$ and ignoring any flow beneath as a useful proxy for surface heights below $y = 0$. The approach is tested in 2D within the context of triple-deck asymptotic theory.

*Graduate Student Researcher, AIAA Student Member
†Professor, Aerospace Engineering, AIAA Associate Fellow

This simple model, perhaps most valid in the limit of very steep and narrow dents, is based the fluid flow moving over the dent with little or no downward deviation of its streamlines. Throughout literature, there are several examples of comparisons between bumps and dips, and how they affect the flow. Bumps consistently have a larger effect on mean flow and stability. El Mistikaway [9] examined elastic humps and dents and found that fluid flow has much less of an effect on the shape of dents. This trend, however, does appear to be affected strongly by roughness slope.

A related approach was used by Gaster [10] to examine the effects of pits on Tollmien-Schlichting stability. He noted two significant trends. First, when the roughness heights were increased, the size of separation regions and the fluid circulation increased. Second, when the peaks were moved closer together, the size of separation regions again increased, but the fluid circulation decreased. He projected that for sandpaper-like roughness the fluid trapped between peaks would be nearly static.

Triple-deck asymptotic theory is used to numerically simulate the boundary-layer. This theory, developed by Lighthill [11], along with Stewartson and Williams [12], was used initially to explain separation of boundary layers in supersonic flow. It shows that by matching layers of different scaling around a disturbance (usually an abrupt change in boundary conditions) boundary-layer theory can be extended to explain scenarios where upstream influence via the pressure is necessary. An interaction between regions of different scalings allows information about disturbances to travel up through the decks to the inviscid outer deck, which in subsonic boundary layers is governed by an elliptic inviscid law.

Numerical development of the theory found that the viscous-inviscid interaction laws allowed for regular integration of boundary layers through regions of small separation bubbles, thereby avoiding Goldstein's singularity [13]. Flow properties can be fully described by numerical solutions of the boundary layer equations coupled to the interaction law of the inviscid, elliptic outer flows. This reduced model allows for simpler computational models when examining disturbances in the boundary layer.

II. Methods

Using the method of matched asymptotic expansions one can identify three distinct regions (or 'decks'), each with their own scaling laws and governing equations. Information about disturbances is propagated upstream by allowing perturbations (in the form of displaced streamlines and localized pressure gradients) to move up and out of the viscous region, then upstream by way of the elliptic inviscid equations outside of the Prandtl boundary layer. Lighthill [11], followed by Stewartson and Williams [12], formulated the correct scaling necessary for creating a consistent approximate solution to the Navier-Stokes equations. Derivation of triple-deck theory shows that the viscous-inviscid interaction region occurs over a length scale of $Re^{-3/8}$. The lower deck is scaled as $Re^{-5/8}$, the middle deck as $Re^{-4/8}$, and the upper deck as $Re^{-3/8}$. These scalings allow different leading order terms to emerge from the Navier Stokes equations, which leads to different governing equations for each deck.

The decks are divided as follows: the lower deck is governed by the incompressible boundary layer equations and is characterized by rotational and viscous disturbances. A passive middle deck exists, still inside the boundary layer, that reacts to disturbances. The characteristic perturbation in the middle deck is the bending of streamlines, a 'displacement' effect. The outer deck, which extends slightly into the freestream, relates displacement and pressure in subsonic flow through the Prandtl-Glauert relationship. This region is inviscid and irrotational.

A. Governing Equations

The lower deck is governed by the incompressible boundary-layer equations.

$$\begin{aligned} u_x + \tilde{v}_{\tilde{y}} &= 0, \qquad \text{and} \\ uu_x + \tilde{v}u_{\tilde{y}} &= p_x + u_{\tilde{y}\tilde{y}} \end{aligned} \tag{1}$$

where a ~ denotes a variable prior to the Prandtl transformation 4 used to model positive height surface bumps. Boundary conditions were either a no-slip boundary condition where the boundary layer moved over solid surfaces or a no-shear condition where the boundary layer was imagined to be moving over an effective surface over a dip in geometry. No penetration was enforced everywhere for the normal component of velocity. As $\tilde{y} \to \infty$, the velocity tends towards the base shear flow plus an additional constant velocity deficit or excess. That velocity 'slip' between the lower deck and main deck corresponds to a displacement which will help dictate the local pressure gradient through the outer deck and inviscid law.

$$
\begin{aligned}
&u(\tilde{y} = h(x)) = 0 \qquad \text{(no slip)} \\
&u_{\tilde{y}}|_{(\tilde{y}=h(x))} = 0 \qquad \text{(no shear)} \\
&\tilde{v}(\tilde{y} = h(x)) = 0 \\
&u(\tilde{y} \to \infty) \to \lambda(\tilde{y} + A(x))
\end{aligned}
\tag{2}
$$

Upstream, far away from the disturbances ($x \to -\infty$), the flow was assumed to have returned to a Blasius flow:

$$
u \to \lambda\tilde{y}, \qquad \tilde{v} \to 0, \qquad p \to 0 \tag{3}
$$

The Prandtl transformation is applied [14] to model positive surface heights:

$$
y = \tilde{y} - h(x), \qquad v = \tilde{v} - uh_x \tag{4}
$$

The boundary layer equations and upstream boundary conditions remain unchanged in this transformation while the wall boundary conditions change to:

$$
\begin{aligned}
&u(y = 0) = 0 \qquad \text{(no slip)} \\
&u_y|_{(y=0)} = 0 \qquad \text{(no shear)} \\
&v(y = 0) = 0 \\
&u(y \to \infty) \to \lambda(y + A(x) + h(x))
\end{aligned}
\tag{5}
$$

The outer deck is governed by the following inviscid law:

$$
p(x) = \frac{1}{\pi}\int_{-\infty}^{\infty} \frac{\delta'(\xi)d\xi}{\xi - x}, \qquad \text{where} \qquad \delta = -A(x) + h(x) \tag{6}
$$

In order to analyze nonlinear heights ($h \sim O(1)$) a numerical simulation was developed using the quasi-simultaneous approach to viscous-inviscid interaction problems developed by Veldman [15].

B. Boundary-layer Solver

For simplicity, the u component of velocity is split into its lower deck components: the perturbation, $\hat{u}$ and the base shear flow, λy. The local shear stress constant λ is taken to be unity without loss of generality [16]. A coordinate stretch $\eta = y/(1 + y)$ is applied in the normal direction to allow a large computational area to closer approximate the conditions as $y \to \infty$, while still tightly clustering grid cells near the wall to capture large gradients. The upper limit of η was generally taken to be 0.95 which corresponds to $y_{max} = 20$. No coordinate stretch was applied in the x direction.

A survey of the literature [15] [17] [18] indicates the necessity for the boundary layer equations to be solved in a coupled fashion. The coupling of momentum and continuity has been found to eliminate oscillations in shear stress in areas of reversed flow. The code used second-order differencing schemes for streamwise derivatives in both the x-momentum and continuity equations, and central differences for all wall-normal derivatives. Newton's method was used to eliminate the non-linearities from the convective terms.

In areas of reversed flow, the scheme needed to be adjusted to allow stable forward integration. As a first approximation, the term uu_x was set to zero whenever $u < 0$. This is known as the FLARE approximation [19]. Due to the iterative nature of inverse methods, after a first sweep had been completed this approximation was replaced by forward differencing in reversed flow using values from past sweeps.

C. Inviscid Law

Equation 6 was first approximated as a finite integral over the computational domain. The finite portion was approximated using the trapezoid rule following the method laid out by Veldman [15].

$$
p_j = \sum_{i=1}^{N_x - 1} \frac{\delta'_{i+1/2}}{i - j + 1/2} \tag{7}
$$

where p is pressure, δ' is $d\delta/dx$, and j is the streamwise station index. Constants spacing in x is assumed in equation 7, where δ' is replaced by a first-order backwards finite difference approximation.

Veldman [20] stresses how the disturbances at a triple-deck scale break down the typical hierarchy of the boundary layer equations. Instead of the direct approach, where a pressure gradient or edge velocity is prescribed, or an inverse procedure, where a displacement thickness is prescribed, Veldman's scheme [15] uses the inviscid law to prescribe a linear combination of pressure and displacement. Equation 7 was incorporated into the boundary layer equations through the following expression:

$$p_j^{n+1} - \alpha_{jj}\delta_j^{n+1} = \sum_{i=2}^{j-1} \alpha_{ij}\delta_i^{n+1} + \sum_{i=j+1}^{N_x-1} \alpha_{ij}\delta_i^{n} \tag{8}$$

where a_{ij} is the coefficients results from expansion of the summation in equation 7. j indicates the streamwise station, and n indicates the iteration count.

The solution was initiated far upstream of the roughness elements in the Blasius region and the solution marched downstream. Using equation 8, pressure at the current x station was eliminated, and the boundary layer equations were solved to yield new velocities, along with the displacement and pressure. Due to the elliptic nature of the incompressible inviscid law, global iterations were required.

$$A(x)^{n+1} = (1-\omega)A(x)^n + \omega A(x)^{n+1} \tag{9}$$

This expression was over-relaxed with $\omega = 1.5$. Convergence was considered to be achieved when $max(|\delta^{n+1} - \delta^n(i)|) < 10^{-5}$.

III. Results

A. Test Cases

To check the code, two test cases were examined. First was the linear bump examined by Smith [16]. The geometry of this bump is:

$$F(x) = hx(1-\theta x)/\theta \qquad \text{for} \qquad 0 \le \theta x \le 1, \qquad \text{and} \qquad F(x) = 0 \qquad \text{elsewhere} \tag{10}$$

where θ is Lighthill's constant, 0.8272. Present results are nearly identical to Smith's, as well as Napolitano et al., who numerically simulated the same geometry [21]. Figure 1 shows the normalized pressure and wall shear stress for $h = 0.1$. Note the inclusion of a local shear stress factor was necessary for comparison.

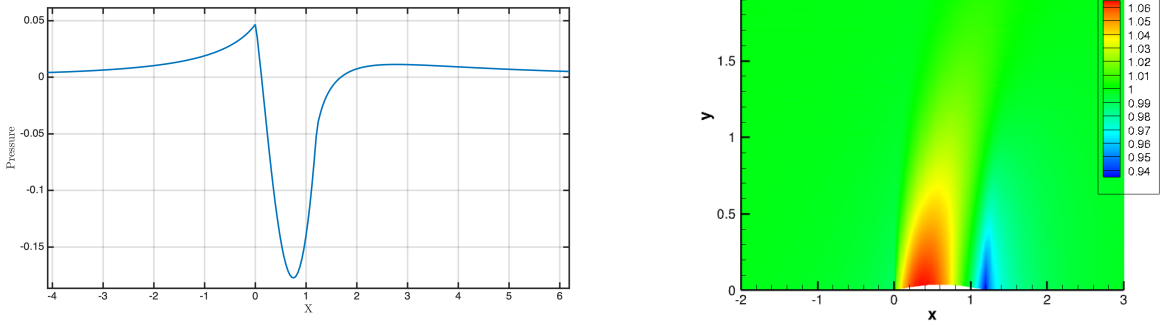

(a) Normalized Pressure

(b) Normalized Shear

Fig. 1 Comparison with Smith's linear bump [16]

Figure 2 shows a streamwise step size convergence study. Both x and y showed approximately first-order behavior.

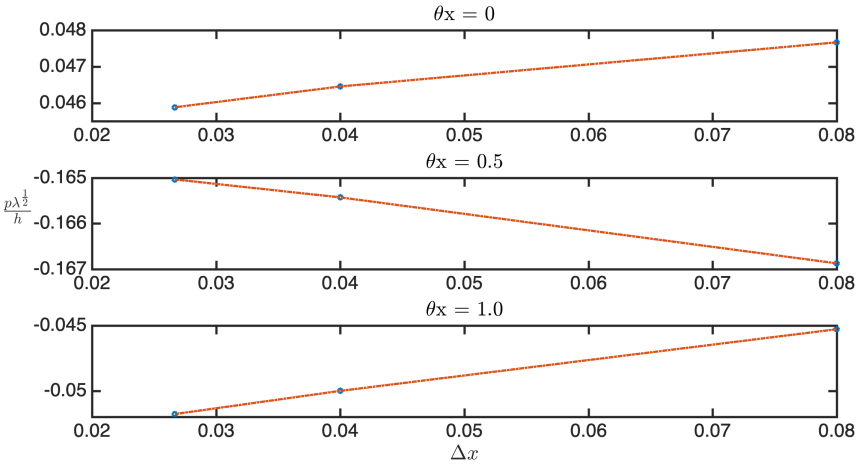

(a) Streamwise Step Size

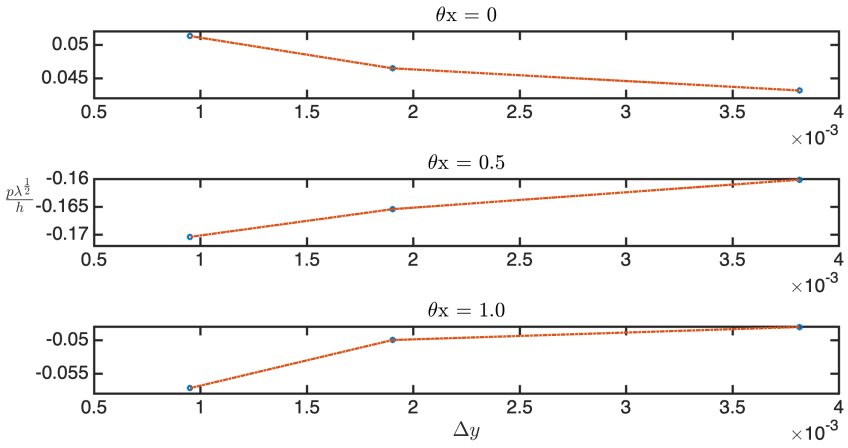

(b) Wall Normal Step Size

Fig. 2 Stepsize Convergence Study

The x and y limits of the computational domain were also extended to ensure there was no effect. The x domain was changed from ±20 to ±25, and the y domain was changed from 20 to 25. Changes were negligible.

The code was also compared against Sykes' quartic bump geometry:

$$F(x) = h(1 - x^2)^2 \qquad \text{for} - 1 \leq x \leq 1, \qquad \text{and} \qquad F(x) = 0 \qquad \text{elsewhere.} \tag{11}$$

Specifically, the performance of the code in regions of separation was examined. There was some discrepancy between the value of h reported by Sykes where separation was first seen ($h \approx 1.9$ for Sykes, vs. $h \approx 1.1$ here), but this is likely due to the exclusion of the local shear stress factor λ. Qualitatively, the separation zone seen in Figure 3 is similar to the separation zone in Sykes paper [22]. The code is able to smoothly integrate through regions of mild separation. At large heights, however, the code did become unstable. This occurred around $h = 2$. This is likely a numerical instability for large separation.

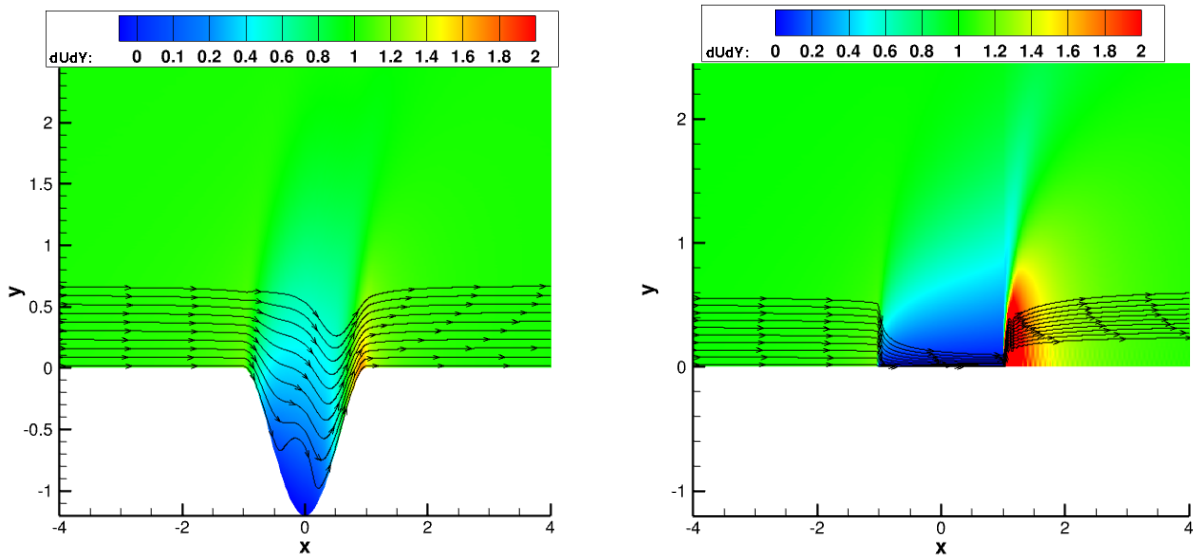

(a) No-Slip Boundary Condition

(b) No-Shear Boundary Condition

Fig. 3 No-slip versus no-shear, Sykes' Quartic Hump, $h = -1.2$

Figure 3 also shows a third test case that compares a surface dip to a no-shear boundary condition above where the dip would lie. There are some oscillations apparent in the wall shear stress after a no-shear region. This is likely numerical and possibly due to the extreme gradients induced by the sudden change in boundary conditions. No correcting factor has yet been added for streamline curvature (a higher order effect [20]), which may resolve this issue.

The no-shear case shows an interesting result. There is a large spike in shear stress after the flow 'reattaches' to the wall. This is explained by the large negative gradient in streamwise velocity caused by the sudden change from no-shear to no-slip. Streamlines stress this discontinuity by exhibiting a large spike in normal velocity. While the spike in shear stress makes sense in the context of the present model, it does not reflect intuition based on experiments for distributed roughness. Such a large disturbance of the flow would have increased the likelihood of transition simply due to the presence of the roughness field.

B. No-shear vs. no-slip

Several additional cases tested the no-shear condition as a proxy for surface dips. Equation 12 was used with positive and negative values of h to switch between the bump-dip-bump case and the dip-bump-dip case, respectively. All results shown use $N_x = 1001$, $N_y = 500$.

$$\begin{aligned} F(x) &= h\sin^2(\frac{\pi}{2}(x+3)) \qquad \text{for} \qquad -3 \le x \le -2 \\ F(x) &= h\sin(\frac{\pi}{2}(x+3)) \qquad \text{for} \qquad -2 < x < 2 \\ F(x) &= h\sin^2(\frac{\pi}{2}(x+3)) \qquad \text{for} \qquad 2 \le x \le 3 \\ F(x) &= 0 \qquad \text{elsewhere} \end{aligned} \tag{12}$$

A height of $h = 0.8$ was selected, based on a separation region appearing for the no-slip case of bump-dip-bump. Based on previous comments about the severity of a bump versus a dip, intuition would suggest the maximum shear stress would be higher for the bump-dip-bump case when a no-slip boundary condition is enforced everywhere. For the bump-dip-bump case, the non-dimensionalzed max shear stress is $\tau = 2.59$. For the dip-bump-dip case, the non-dimensionalized max shear stress is $\tau = 2.47$. Similarly, the maximum adverse pressure gradient was higher for the bump-dip-bump case, at $dp/dx = 0.90$ versus $dp/dx = 0.78$ for the dip-bump-dip case. Figures 4 and 5 shows the streamlines, shear stress, and pressure for the bump-dip-bump and dip-bump-dip cases, respectively.

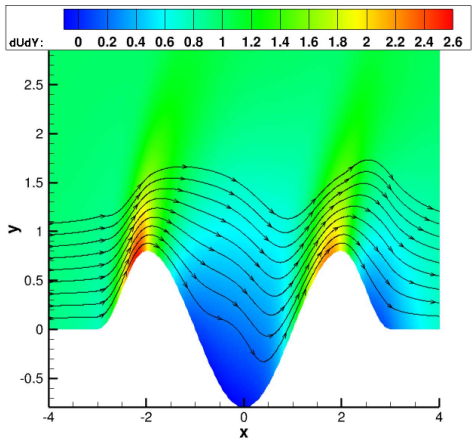

(a) Shear Stress - $\frac{dU}{dY}$

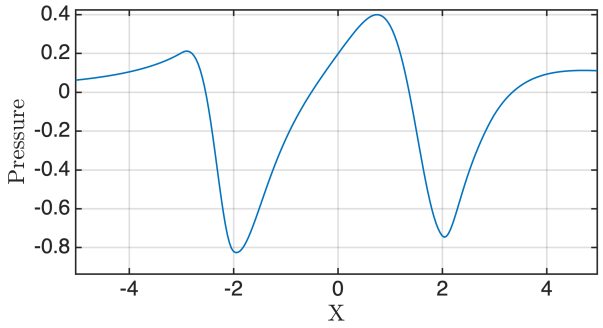

(b) Pressure

Fig. 4 Bump - Dip - Bump; No-Slip Bounary Conditions

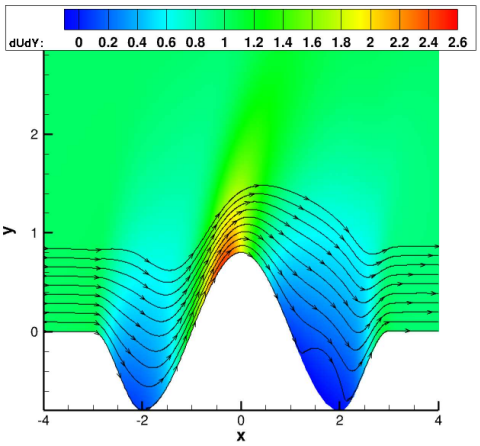

(a) Shear Stress - $\frac{dU}{dY}$

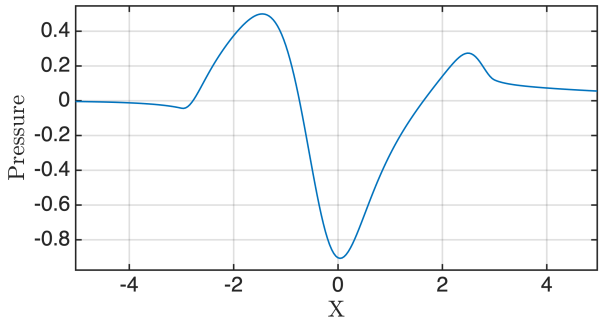

(b) Pressure

Fig. 5 Dip - Bump - Dip; No-Slip Bounary Conditions

Next, a no-shear condition was enforced for the same geometries wherever $y_{physical} < 0$. Figures 5 and 6 shows the streamlines, shear stress, and pressure for the bump-dip-bump and dip-bump-dip cases, respectively. Note the maximum shear stress is displayed on the same scale as the no-slip cases.

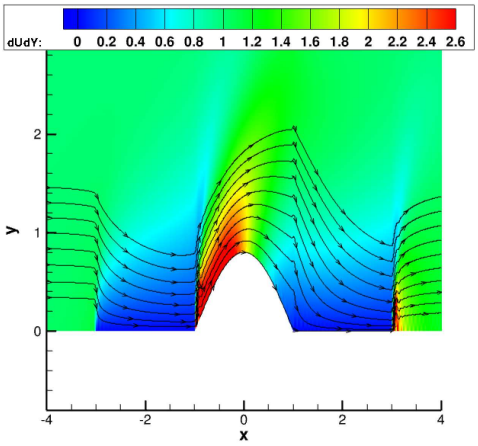

(a) Shear Stress - $\frac{dU}{dY}$

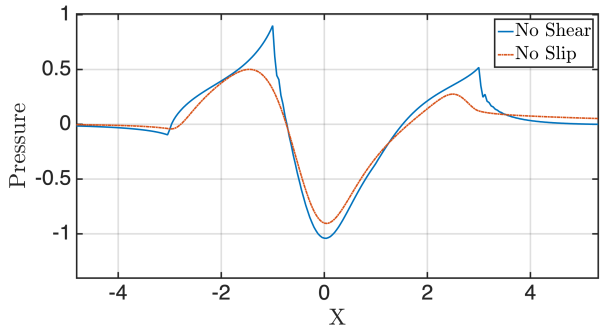

(b) Pressure

Fig. 6 Dip - Bump - Dip; No-Shear Bounary Conditions

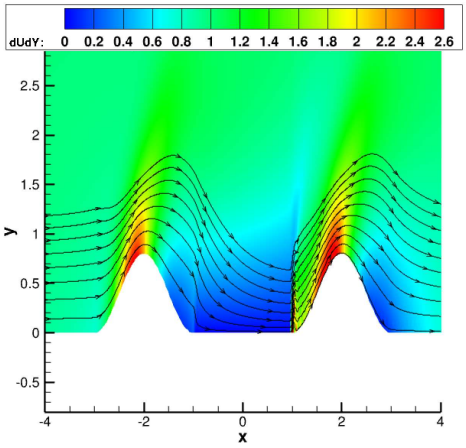

(a) Shear Stress - $\frac{dU}{dY}$

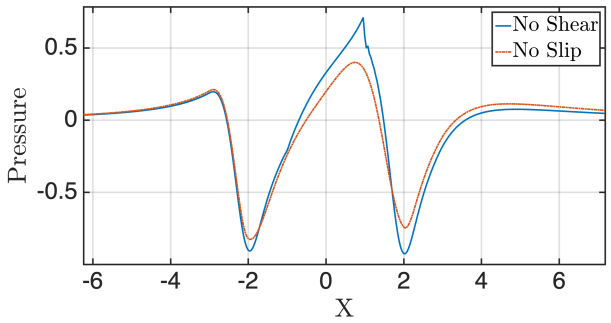

(b) Pressure

Fig. 7 Bump - Dip - Bump; No-Shear Bounary Conditions

These cases show the same trend as the original test case. There is a large spike in shear stress immediately after 'reattaching' due to the large negative gradient in streamwise velocity. For these cases, the shear returns to no-slip levels quickly.

Additionally, the maximum shear stress is significantly higher for the dip-bump-dip case, opposite of what was observed in the no-slip simulations. For the dip-bump-dip case, maximum non-dimensionalized shear stress is $\tau = 7.78$, versus $\tau = 4.84$ for the bump-dip-bump case. This can be also be explained reasonably in the context of the no-shear model. For the bump-dip-bump case, as the flow approaches the no-shear region, it is moving slower than the base flow due to the presence of the first bump. When it accelerates of the no-shear region, it can't reach as high of a velocity as the dip-bump-dip case. In that scenario, the fluid has not yet been perturbed from the base flow, and so has a higher velocity near the wall.

A final case was considered where the effective slip surface was raised above $y = 0$. Figure 8 shows the streamlines, shear stress, and pressure.

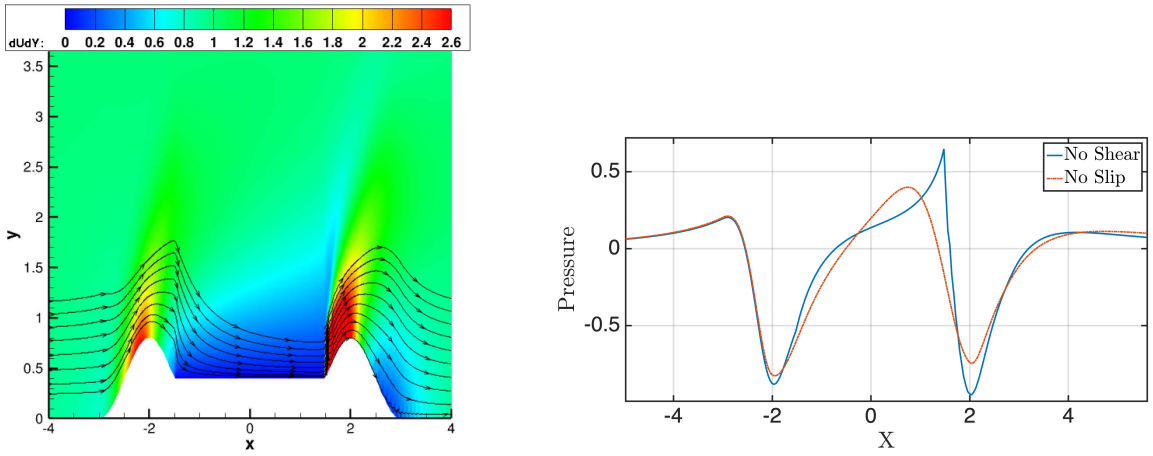

(a) Shear Stress - $\frac{dU}{dY}$

(b) Pressure

Fig. 8 Bump - Dip - Bump; No-Shear Bounary Conditions. Y_{eff} Raised

This case results in the highest shear stress seen, with a maximum non-dimensionalized shear stress of $\tau = 9.89$. Again, this is reasonable in the context of the no-shear model. Because the no-shear surface has been raised, it is effectively longer in the streamwise direction. The flow spends a longer time accelerating in the no-shear region, and is subjected to a larger velocity gradient upon reattaching.

IV. Conclusions and Future Work

The purpose of this paper was to examine a no-shear boundary condition at $y = 0$ as a first approximation for locations at which distributed roughness dips beneath $y = 0$. While the results of the model are consistent with an intuitive analysis of fluid flow under no-shear conditions, they do not yet adequately match experimental evidence for fluid flow over distributed roughness. The large spike in shear stress where slip boundaries transition to no-slip boundaries suggest a more sophisticated approach is needed.

For insight on future attempts, we can return Gaster's comments on fluid recirculation between roughness peaks. The speed of the fluid in the gaps is dependent on roughness height and the wavelength of Gaster's periodic roughness. This recirculating fluid must be driven by some outside force to continue its movement against the loss of energy from friction at the wall. Viewed through this lens, the fluid riding above the effective surface must impart *some* shear force for compatibility with the fluid below. A combination of no-shear and no-slip along the effective surface appears necessary and will be the direction of continuing efforts.

V. Acknowledgments

This work is supported by NSF Grant CBET-1805889.

References

[1] Tani, I., "Boundary-layer transition," *Annual Review of Fluid Mechanics*, Vol. 1, No. 1, 1969, pp. 169–196.

[2] Nikuradse, J., "Laws of flow in rough pipes," *VDI Forschungsheft*, 1933, p. 361.

[3] Reshotko, E., and Leventhal, L., "Preliminary Experimental Study of Disturbances in a Laminar Boundary Layer Due to Distributed Surface Roughness," *AIAA Paper 81-1224*, 1981.

[4] Kendall, J., "Laminar boundary layer velocity distortion by surface roughness: Effect upon stability," *AIAA Paper 81-0195*, 1981.

[5] Drews, S., Downs III, R. S., Doolittle, C., Goldstein, D., and White, E., "Direct numerical simulations of flow past random distributed roughness," *AIAA Paper 20110564*, 2011.

[6] Downs, R. S., White, E., and Denissen, N., "Transient Growth and Transition Induced by Random Distributed," *AIAA Journal*, Vol. 46, No. 2, 2008, pp. 451–462.

[7] Kuester, M. S., and White, E. B., "Roughness receptivity and shielding in a flat plate boundary layer," *Journal of Fluid Mechanics*, Vol. 777, 2015, pp. 430–460.

[8] McMillan, M. N., Berger, A. R., and White, E. B., "Measurements of Distributed Roughness Receptivity," *AIAA Paper 2017*, 2017.

[9] El-Mistikaway, M. A., T., "Subsonic triple deck flow past a flat plate with an elastic stretch," *Applied Mathematical Modeling*, Vol. 34, No. 5, 2010, pp. 1238–1246.

[10] Gaster, M., "Understanding the effects of surface roughness on the growth of disturbances," *AIAA Paper 2016*, 2016.

[11] Lighthill, M. J., "On boundary layers and upstream influence II," *Proc. R. Soc. Lond*, Vol. A217, No. 478, 1953.

[12] Stewartson, K., and Williams, P., "Self-induced separation," *Proc. R. Soc. Lond.*, Vol. A312, No. 181, 1969.

[13] Goldstein, S., "On Laminar Boundary Layer Flow Near A Position Of Separation," *The Quarterly Journal of Mechanics and Applied Mathematics*, Vol. 1, No. 1, 1948, pp. 43–69.

[14] Van Dyke, M., "Laminar Boundary Layers. Edited by L. Rosenhead. Oxford University Press, 1963. 688pp. aE4. 10s." *Journal of Fluid Mechanics*, Vol. 18, No. 3, 1964, p. 477–480.

[15] Veldman, E. P., A., "The calculation of incompressible boundary layers with strong viscous-inviscid interaction," *NASA STI/Recon Technical Report N*, Vol. 81, 1980.

[16] Smith, F. T., "Laminar flow over a small hump on a flat plate," *J. Fluid Mech.*, Vol. 57, No. 4, 1973, pp. 803–824.

[17] Pletcher., H., R., Tannehil, C., J., and Anderson, A., D., *Computational Fluid Mechanics and Heat Transfer*, CRC Press LLC, 2013.

[18] Carter, E., J., and Wornom, F., S., "Forward marching procedure for separated boundary-layer flows," *AIAA Journal*, Vol. 13, No. 8, 1975, pp. 1101–1103.

[19] Reyhner, A., T., and Flügge-Lotz, I., "The interaction of a shock wave with a laminar boundary layers," *International Journal of Non-Linear Mechanics*, Vol. 3, No. 2, 1968, pp. 173 – 199.

[20] Veldman, A., "Matched asymptotic expansions and the numerical treatment of viscous-inviscid interaction," *Journal of Engineering Mathematics*, Vol. 39, No. 1, 2001, pp. 189–206.

[21] Napolitano, M., Werle, J., M., and Davis, T., R., "Numerical Technique for the Triple-Deck Problem," *AIAA Journal*, Vol. 17, No. 7, 1979.

[22] Sykes, I., R., "Stratification effects in boundary layer flow over hills," *Proceedings of the Royal Society of London,*, Vol. 361, 1978, pp. 225–243.